Energetic convenience of cell division in biological tissues

Marco Picchi Scardaoni [*]

Department of Civil and Industrial Engineering, University of Pisa, Largo Lucio Lazzarino 2, 56122 Pisa, Italy

A typical feature of living tissues is proliferation by division: it is a fundamental aspect of many biological processes, including embryonic development, morphogenesis, and cancer growth. Here, we study the energetics of cell division occurring in epithelia, highlighting the interplay of the key parameters ruling mitosis. We find the existence of a region, in the parameter space, which is independent of the cell elasticity and weakly dependent on the ratio between mother and daughter cells areas. In this region, cell division is energetically favorable. Our results may lead to an exact characterization of cells having anomalous proliferation.

I. INTRODUCTION

One of the features characterizing living tissues is the capability to grow and to adapt their topology when necessary. Specifically, cells can undergo topological changes during their life. The most important are, probably, the T1 transition and mitosis, i.e., the process by which a single mother cell divides into two daughter cells.

In the T1 transition, cells manage to change neighboring cells, thus promoting motility and migration within the tissue. This transition has been widely studied in the literature. For instance, it is responsible for pattern creation or for the emergence of compartments of cells of the same type in heterogeneous tissues. It has been shown that to activate such transformations, an energy barrier must be overcome. If this is the case, the tissue eventually moves towards a new local energy minimum [1,2]. Moreover, a simple but striking connection between the energy barrier amount, the transition between a solidlike (or glassy) behavior towards a fluidlike response, and the isoperimetric inequality has been found in [1–7]. This represents a paradigmatic example of the interplay between geometry, mechanics, and biology. Although we can assert that the T1 transition is quite understood, it is not the case for mitosis.

Despite the advanced understanding of cell physiology, there is still no quantitative connection between the mechanical and geometrical parameters ruling the process. This work aims at shedding light on these aspects, trying to bridging the gap in the scientific literature. In particular, we aim at identifying (i) the leading parameters driving mitosis, from a joint mechanical and geometrical setting and at showing their interplay; (ii) under which conditions mitosis shall be sustained by energy supply, i.e., the presence of an energy barrier to overcome; and (iii) under which conditions cell division, hence proliferation, is energetically favorable, in the sense that the energy state of the tissue after the division is lower.

It will come as no surprise that we approach this problem from a geometric and mechanical viewpoint. A wide literature, especially in recent years, has been produced on this topic. For instance, the connection between growth and internal stress is well established [8–10]. It has been shown that the internal stress can modulate the growth-preferred directions, providing an effective (re)modeling tool to the growing body [11,12]. We remark that, however, the definition of growth is not univocal among different scientific communities. From a continuum mechanics point of view, growth is generally synonymous with bulk (or volumetric) growth. The volumetric growth of a soft elastic tissue is the change in the local stress-free state without requiring the existence of a corresponding global stress-free configuration [10,13–15]. Hence, growth is linked to the geometrical incompatibility of the current configuration.

More important for our goal is that the stress level within a cell regulates the rate of cell proliferation and growth. There exists a homeostatic pressure that balances and regulates cell proliferation and death [16–18]. Healthy cells have a (chemo)mechanical feedback system regulating the biological functionalities. On the contrary, malignant cancerous cells have lost the ability to self-regulate, and they duplicate in an uncontrolled manner [19,20]. From these considerations, the deep interdisciplinary connections between mitosis, cancer proliferation, biology, mechanics, and geometry are evident.

The geometry (shape) and the mechanic response of a generic body are generally encapsulated within an energy functional. This is also the case for cellular tissues, where an energy expression, borrowed from the vertex model methods [21,22], has been widely employed for numerical and theoretical predictions. The vertex model, in its simplest essence, considers a tiling of the plane (even though three-dimensional vertex models have been developed) where every polygonal tile represents a cell. A simple yet nontrivial potential energy is associated with each cell. The energy takes into account the elasticity of the cytoskeleton, of the actomyosin ring contractility, and of the adhesion between cells. At each vertex of the tessellation, a net force is exerted, according to a dynamical law relating the evolution of the vertices positions and the

---

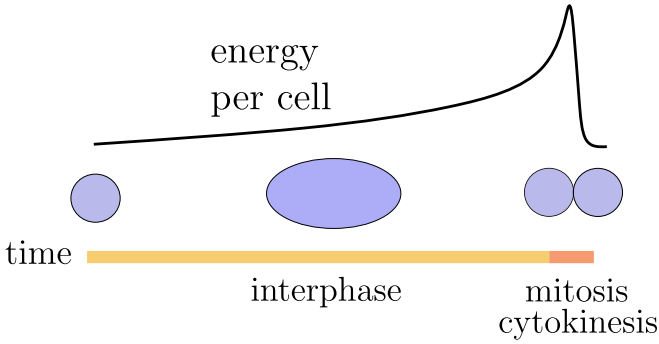*marco.picchiscardaoni@ing.unipi.it

054405-1

FIG. 1. Cartoon of cell cycle, adapted from [35]. The (qualitative) energy curve refers to the mother cell before division and to a single daughter cell after division.

total energy. We emphasize that the major achievements on T1 transitions and cellular tissues in general, both numerical and analytical, have been obtained starting from the energy expression employed in vertex models, with excellent agreement with the experiments [1,4,6,23]. In this work, we will consider the same starting point.

Within the vertex model methods, cell division is difficult to handle due to the modification of the original tiling [24]. That is, artificial treatments are required for numerical simulations in these models. It is usually assumed that when cells undergo mitosis, they split into two equal areas [24,25], and the modeling reduces to a mere geometrical consideration. In particular, the criterion triggering cell division is the attainment of a certain critical area [26]. In so doing, cell division is always prompted by the algorithm, regardless of any energetic consideration. Clearly, the way cells divide geometrically [27–29] and the rate at which they do so [30,31] strongly affect the final topology and microstructure (internal reorganization) of the tissues. What is missing is an energetic point of view on mitosis.

What do we know about the relationship between cell division and bioenergetics? Cell division is indeed a complex process with substantial energy demands, and how cells regulate the generation of the required energy is still not well understood. However, many studies suggest a connection between cell division and their metabolism [32].

The complete process of cell reproduction is called the *cell cycle*, intuitively depicted in Fig. 1. For reasons we do not need to specify, a quiescent cell starts to grow (*interphase*). In this phase, the cell duplicates DNA and other genetic material. At a critical point, if some *checkpoints* [33] to verify the integrity of the major events of the cell cycle are satisfied, the mother cell enters in the properly named *mitosis* phase, and two daughter cells are generated by abscission (*cytokinesis*). The daughter cells may possibly enter in turn in a cell cycle. Usually, the mitotic phase represents less than 10% of the whole cell cycle [34].

In a recent paper [35], the authors studied the mitochondrial bioenergetics, at the single-cell level, for the whole cell cycle. Specifically, they managed to measure the mitochondrial membrane potential in murine lymphocytic leukemia cells. They found a monotonic trend during the interphase, with an important increase of energy at the beginning of the

mitotic phase. In the second part of mitosis, energy decreases approximately up to the original maternal level (see, in particular, Figs. 1(a), 1(e) and 1(g) of [35]). A qualitative energy trend, adapted from these findings, is reported in Fig. 1.

Needless to say, the biological cell division is promoted by many complex, interrelated phenomena of a different nature, i.e., chemical, biophysical, etc., so that "energy" contains many contributions. In what follows, as anticipated, we will assume a pure mechanical-geometrical viewpoint. Note that this is a customary framework in which to study tissue and cellular evolution. As reported in [33], shape is recognized to play an important role in cell division. To maintain cell size and ensure that daughter cells are endowed with the appropriate amount of genetic material, cells must, on average, double their contents before division. Control of cell size is critical for regulating nutrient distribution for the cell, and regulating organ size and function in multicellular organisms. The mechanical-geometrical viewpoint is thus not without merit.

The paper is structured as follows. Section II states the main assumptions of our investigation, and it contains the theoretical parts of the paper together with the principal findings. In particular, Sec. II A introduces the theoretical framework that will be used in the paper, stating the main assumptions; Sec. II B analyzes the case of equal splitting of the mother cell, leading to the existence of a region of energetic convenience for division; Sec. II C investigates the cases in which the mother cell does not divide equally; and Sec. II D generalizes some of the previous results for the growing cell. Section III presents five simulations using a simple, in-house vertex model implementation. The results are consistent with the theoretical and experimental evidence. Section IV shows, under some optimality assumptions, the complete history of the growth and division of a cell. The energy profile is consistent with experimental observations. Finally, Sec. V concludes the paper with meaningful remarks and prospects.

II. ENERGETICS OF CELL DIVISION

A. Theoretical setting

For a cell, we consider the well-known energy adopted in vertex model approaches [21,22,24,25,36]:

$$E_1 := K_A(A - A_0)^2 + K_P(P - P_0)^2. \tag{1}$$

The first term represents the elasticity of the cytoskeleton. A is the current area of the generic cell, and A_0 is the target area. K_A is the area modulus. Similarly, the second term models actomyosin ring contractility and adhesion between cells. P is the current perimeter, and P_0 is the target perimeter. K_P is the perimeter modulus. For the time being, we regard these quantities as positive constants.

We have already mentioned that the mitotic phase, experimentally, is much shorter than the growth interphase. Ideally, we may assume that mitosis occurs instantaneously. On this basis, we can compare the cell energies astride two instants: just before and just after the division. After a single division,
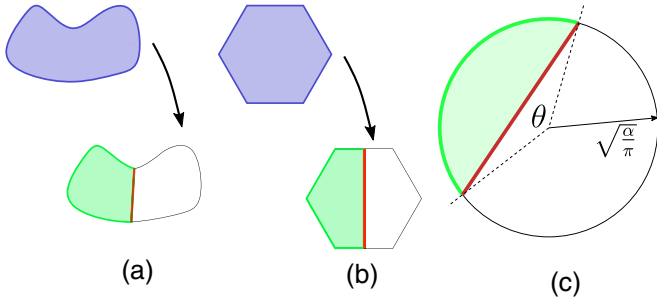
FIG. 2. Cell division cartoon. (a) A cell of area α and perimeter p divides into two cells via the creation of a new surface of size ℓ. The original area splits into α_1 and $\alpha - \alpha_1$, the original perimeter into p_1 and $p - p_1$. (b) Regular hexagon case. The new surface equals twice the apothem of the polygon. (c) Circular cell of area α undergoing nonequal division.

the energy of the two daughter cells reads

$$E_2 := K_A(A_1 - A_0)^2 + K_A(A - A_1 - A_0)^2 +$$
$$+ K_P(P_1 + L - P_0)^2 + K_P(P - P_1 + L - P_0)^2, \quad (2)$$

where L is the length of the new surface, which materially divides the mother cell into two parts. In writing (2), we have assumed that the original area A is split into two parts, namely A_1 and $A_2 = A - A_1$, as well as the original perimeter P. We have also assumed that the daughter cells inherit the same elastic moduli and target area and perimeter from the mother cell. It is easy to see that the energy of possible surrounding cells is not affected astride the division instant. Given this local property of mitosis, both in space and time, we can study the division of one cell without loss of generality.

We seek conditions in which the cell division is energetically favorable, i.e., conditions in which $E_2 - E_1 \leqslant 0$. A direct computation shows that

$$E_2 - E_1 = K_A\left(A_0^2 + 2A_1^2 - 2AA_1\right) + K_P\left(P_0^2 + 2P_1^2 - 2PP_1\right)$$
$$+ 2K_P L(L + P - 2P_0). \quad (3)$$

We assume $\sqrt{A_0}$ to be a characteristic size of the cell, and we rescale the energy difference (3) by $K_A A_0^2$. Accordingly, the dimensionless energy difference can be rewritten as

$$\Delta E := \frac{E_2 - E_1}{K_A A_0^2} = \left(1 + 2\alpha_1^2 - 2\alpha\alpha_1\right)$$
$$+ K\left(s_0^2 + 2p_1^2 - 2pp_1\right)$$
$$+ 2K\ell(\ell + p - 2s_0), \quad (4)$$

where we defined

$$K := \frac{K_P}{K_A A_0}, \quad \alpha := \frac{A}{A_0}, \quad \alpha_1 := \frac{A_1}{A_0},$$
$$s_0 = \frac{P_0}{\sqrt{A_0}}, \quad p := \frac{P}{\sqrt{A_0}}, \quad p_1 := \frac{P_1}{\sqrt{A_0}}, \quad \ell := \frac{L}{\sqrt{A_0}}.$$

It is well known that s_0 rules the fluid-solid transition of the mechanical response. This parameter is known in the literature as the *target shape parameter*.

A schematic representation of cell division in reported in Fig. 2(a).

To perform computations, in the spirit of the vertex model method, we hereafter consider n-gonal cells, where $n \in [3, \infty]$ in the number of edges. We recall that the isoperimetric inequality for n-gons reads

$$\frac{P}{\sqrt{A}} \geqslant \sqrt{4n \tan \frac{\pi}{n}} =: q_n,$$

the equal sign holding only for regular ones. In our setting, the isoperimetric inequality states a condition that any realizable n-gon must satisfy. The limit values for q_n are given by triangles, $q_3 := 4.559$, and by circles, $q_\infty = 3.545$. For regular n-gons, we have also

$$a_n = \sqrt{\frac{\alpha}{n \tan \frac{\pi}{n}}} = \frac{2\sqrt{\alpha}}{q_n}, \quad r_n = \sqrt{\frac{2\alpha}{n \sin \frac{2\pi}{n}}} = \frac{a_n}{\cos \frac{\pi}{n}},$$

as the dimensionless apothem and circumradius, respectively.

We further assume that the division surface is actually a straight line.

B. Equal division

In this section, we add the hypotheses that the mother cell is a regular n-gon that splits into two equal parts. Note that the roughly equal splitting is observed also in experimental data (see, for instance, [33]). Accordingly, we have $\alpha_1 = \frac{\alpha}{2}$, $p_1 = \frac{p}{2}$, $p = q_n\sqrt{\alpha}$. Moreover, the division surface passes through the center of the polygon and $2a_n \leqslant \ell \leqslant 2r_n$.

Supposing the division is realized along the shortest segment, we have

$$\ell = \begin{cases} 2a_n = \frac{4\sqrt{\alpha}}{q_n}, & n \text{ even,} \\ a_n + r_n = \frac{2\sqrt{\alpha}}{q_n}\left(1 + \frac{1}{\cos\frac{\pi}{n}}\right), & n \text{ odd.} \end{cases}$$

For cases of major interest, say $n \geqslant 5$, we can actually take $\ell \approx 2a_n$ for *all* values of n, so that

$$\Delta E = \left(1 - \frac{\alpha^2}{2}\right) + K\left(s_0^2 - \frac{q_n^2\alpha}{2}\right)$$
$$+ 2K\frac{4\sqrt{\alpha}}{q_n}\left(\frac{4\sqrt{\alpha}}{q_n} + q_n\sqrt{\alpha} - 2s_0\right). \quad (5)$$

We remark that (5) is exact for any even value and for sufficiently large values of n. The result of our assumptions is depicted in Fig. 2(b) for a hexagon.

For $K = 0$, the unique solution of $\Delta E < 0$ is $\alpha > \sqrt{2}$, independent from the other parameters. $K \to 0$ corresponds to the "incompressible" regime in the following sense: the area term in (1) is preponderant with respect to the perimeter counterpart ($K_P \ll K_A A_0$), so that a cell tends to satisfy (and, possibly, maintain) the condition $A \cong A_0$ to minimize its energy. The reason why $\alpha = \sqrt{2}$ appears as a threshold also has the following interpretation, which does not need the *a priori* assumption of equal splitting. For $K = 0$, (5) simplifies into $\Delta E = 1 + 2\alpha_1^2 - 2\alpha\alpha_1$. Optimizing with respect to α_1, we obtain $\alpha_1 = \frac{\alpha}{2}$ and $\Delta E = 1 - \frac{\alpha^2}{2}$. Imposing $\Delta E = 0$, we find $\alpha = \sqrt{2}$. Thus, the factor $\sqrt{2}$ comes directly from the optimality of equal splitting of the cell.

For $K > 0$, the zeros of (5) can be computed numerically. The results are plotted in Figs. 3(a) and 3(b) for hexagons and
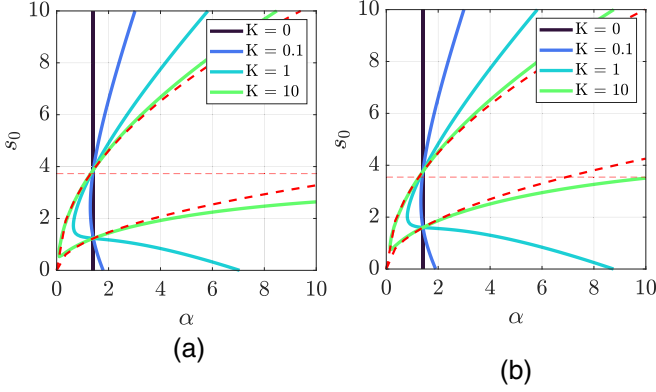
FIG. 3. Zeros of (5) for different K: (a) hexagonal cells, (b) circular cells. Red, dashed curves correspond to $K = \infty$.

circles, respectively. The energetically favorable domain is on the right side of any curve. The horizontal red dashed lines represent the values $s_0 = q_n$. From the plots in Fig. 3 we can identify a limit curve delimiting the favorable region for K sufficiently large (approx. >10). The two limit curves can be determined analytically:

$$\frac{s_0}{\sqrt{a}} = \frac{16 \pm \sqrt{2}\, q_n^2 \mp 8\sqrt{2}}{2\, q_n}. \tag{6}$$

They are represented by red-dashed curves in Figs. 3(a) and 3(b). This case corresponds to considering only the perimeter term in (1). Note that $\frac{s_0}{\sqrt{a}} = \frac{P_0}{\sqrt{A}}$ correlates the target perimeter and current area, in contrast with the T1 transition that is regulated by s_0, a parameter involving only target quantities.

For incompressible cells, the whole region $\alpha > \sqrt{2}$ is energetically favorable. The effect of compressibility is twofold. On the one hand, the energetically favorable domain for $\alpha > \sqrt{2}$ shrinks between the limit curves (6). On the other hand, the domain for $\alpha < \sqrt{2}$ increases in the glassy domain $s_0 < q_n$. The trend is qualitatively the same for hexagonal and circular cells. Note that circular cells present a narrower favorable domain, so that the results for circles are valid also for regular polygons.

It is noteworthy that the region

$$\mathcal{A}_n := \left\{ (\alpha, s_0) \,|\, \alpha > \sqrt{2}, \right.$$

$$\left. \frac{16 - \sqrt{2}\, q_n^2 + 8\sqrt{2}}{2\, q_n} < \frac{s_0}{\sqrt{a}} < \frac{16 + \sqrt{2}\, q_n^2 - 8\sqrt{2}}{2\, q_n} \right\} \tag{7}$$

is energetically favorable for cell division regardless of the value of K. A fortiori, the region A_∞ is energetically favorable also regardless of the number of edges, since $\mathcal{A}_\infty \subset \mathcal{A}_n$ for every n. We have hence shown the existence of a region in the (α, s_0) plane in which mitosis is energetically favorable regardless of the shape and the elasticity of the cells.

We summarize this result in the following.

Proposition 1. Let ΔE, as in (4), be the energy difference of a regular, n-gonal cell undergoing equal division, the segment of separation being the diameter of the incircle. Then, if $(\alpha, s_0) \in \mathcal{A}_\infty$ [see Eq. (7)], $\Delta E < 0$ and the division is energetically favorable.

The converse is not true, in the sense that the actual favorable region can be wider than $\mathcal{A}_\infty$, but it depends on K and n, while $\mathcal{A}_\infty$ does not.

If we additionally require that the initial configuration is stress-free, we have $\alpha = 1$, $q_n = s_0$, so that $\Delta E = \frac{1}{K} + s_0^2 + \frac{64}{s_0^2} - 16$. The inequality $\Delta E < 0$ is never satisfied, as can be inferred by looking at Fig. 3. The interpretation is straightforward: for a stress-free configuration, division is never convenient. In fact, the cell would necessarily move from a zero-energy state towards a higher-energy one.

C. Unequal division

In the previous section, we have considered the ideal case of equal splitting of the mother cell. Now, we investigate the effect of unequal division, i.e., when the mother cell does not split into two identical daughter cells. In the spirit of the previous observations, we consider a circular cell of area α, as shown in Fig. 2(c).

We recall that for a circular cell, $q_n = q_\infty = 2\sqrt{\pi}$ so that $p = 2\sqrt{\pi\alpha}$. Let $\theta \in (0, \pi)$ be the central angle subtending a generic chord ℓ. We can express the geometrical parameters describing the division in terms of this angle, so that

$$\ell = \sqrt{\frac{\alpha}{\pi}}\sqrt{2(1 - \cos\theta)},$$

$$p_1 = \sqrt{\frac{\alpha}{\pi}}\theta, \quad \alpha_1 = \frac{\alpha}{2\pi}(\theta - \sin\theta).$$

Hence

$$\Delta E = \left(1 + \frac{\alpha^2}{2\pi^2}(\theta - \sin\theta)^2 - \frac{\alpha^2}{\pi}(\theta - \sin\theta)\right) + K\left(s_0^2 + 2\frac{\alpha}{\pi}\theta^2 - 4\alpha\theta\right)$$

$$+ 2K\sqrt{\frac{\alpha}{\pi}}\sqrt{2(1 - \cos\theta)}\left(\sqrt{\frac{\alpha}{\pi}}\sqrt{2(1 - \cos\theta)} + 2\sqrt{\pi}\sqrt{\alpha} - 2s_0\right). \tag{8}$$

For $\theta = \pi$, we obtain the case already studied, while for $\theta = 0$ no division occurs. Some solutions to (8) are depicted in Fig. 4 for four values of θ. The horizontal dashed red line represents the value $s_0 = q_\infty$. The trends are similar to those already

discussed for equal division. The unequal division shrinks the domain of energetic convenience and translates it towards larger area ratios and smaller shape parameter values. In fact, not only do the limit curves become closer, but also the solu-
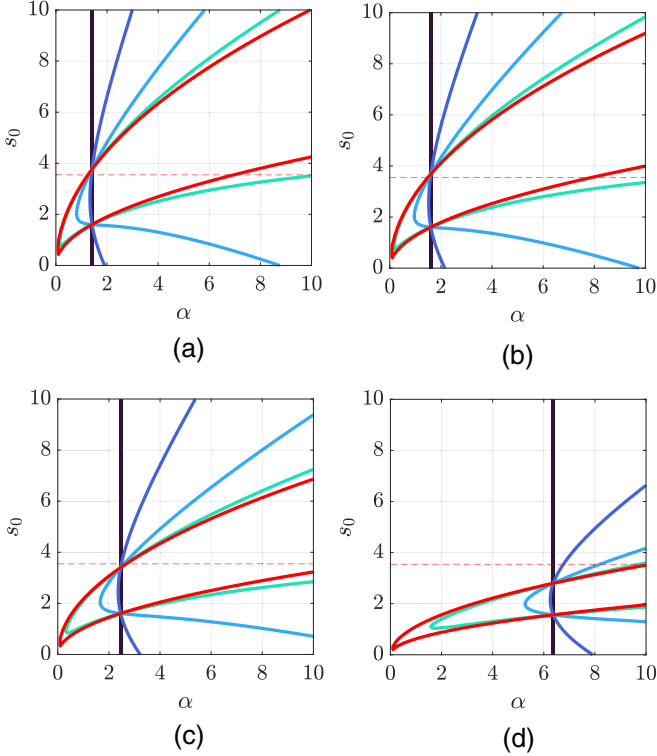
FIG. 4. Zeros of (8) for different K: (a) $\theta = \pi$ ($\frac{\alpha_1}{\alpha} = 0.5$); (b) $\theta = \frac{3\pi}{4}$ ($\frac{\alpha_1}{\alpha} = 0.26$); (c) $\theta = \frac{\pi}{2}$ ($\frac{\alpha_1}{\alpha} = 0.09$); (d) $\theta = \frac{\pi}{4}$ ($\frac{\alpha_1}{\alpha} = 0.01$).

tion for $K = 0$ moves toward higher values of α. This effect is more pronounced for smaller θ. That is, the domain shrinking is more effective when the mother cell divides into strongly dissimilar parts. Moreover, we remark that equal division has more chances to be convenient in the fluid regime $s_0 > q_\infty$, while the unequal division can represent the only possibility in the glassy regime ($s_0 < q_\infty$), at least for a large interval of α [see Figs. 4(c) and 4(d)]. It is remarkable that, neglecting pathological cases in which a cell divides excessively disproportionately, the favorable region for division is quite robust for deviations of $\frac{\alpha_1}{\alpha}$ from the ideal value 0.5 [compare, for instance, Figs. 4(a) and 4(b)]. Hence, for a wide class of cases in which the two daughter cells are not extremely different (these are likely to be the most frequent cases occurring in actual cells), the expression for $\mathcal{A}_\infty$ is still meaningful.

D. Division and growth

So far, we have regarded A_0 as a constant: cells relax substantially. To include cellular growth effects, it is customary in the vertex model literature to consider time-varying reference areas. To generalize our results to take into account cellular growth, we basically substitute the term A_0 appearing in (1) (and the following equations) by the term A_{0t}, representing a target area that can evolve in time t through some specified law. We require only that A_{0t} be of the form $A_0 f(t - \tau)$, where τ is the time when the cell first appears in the tissue and f is some positive function of time such that $f(0) = 1$. A_0 assumes now the meaning of target area for "newly born" cells. Clearly, if A_{0t} does not depend on time, $A_{0t} \equiv A_0 = \text{const}$,

and the cases considered in the previous subsections are fully recovered. Following the assumptions and the logical flow as in Sec. II A, we obtain

$$E_1 = K_A(A - A_{0t})^2 + K_P(P - P_0)^2,$$

$$E_2 = K_A(A_1 - A_0)^2 + K_A(A - A_1 - A_0)^2$$
$$+ K_P(P_1 + L - P_0)^2 + K_P(P - P_1 + L - P_0)^2.$$

Note that the daughter cells inherit A_0 as the target area when they are created. Still assuming $\sqrt{A_0}$ as a characteristic length of the cell, we obtain by nondimensionalization

$$\Delta E := (1 - \alpha_1)^2 - (\alpha - \alpha_{0t})^2 + (1 - \alpha + \alpha_1)^2$$
$$+ K\left(s_0^2 + 2p_1^2 - 2pp_1\right) + 2K\ell(\ell + p - 2s_0),$$

where $\alpha_{0t} := \frac{A_{0t}}{A_0}$. Note that the fourth and fifth brackets are unchanged with respect to the counterpart Eq. (4). Supposing a regular n-gonal cell and equal splitting, we obtain the counterpart of Eq. (5):

$$\Delta E = \frac{1}{2}(\alpha - 2)^2 - (\alpha - \alpha_{0t})^2$$
$$+ K\left(s_0^2 - \frac{q_n^2 \alpha}{2}\right) + 2K\frac{4\sqrt{\alpha}}{q_n}\left(\frac{4\sqrt{\alpha}}{q_n} + q_n\sqrt{\alpha} - 2s_0\right),$$

from which we easily deduce the favorable region, still denoted by $\mathcal{A}_n$,

$$\mathcal{A}_n = \left\{ (\alpha, s_0) \,|\, \alpha > (2 - \sqrt{2})(\alpha_{0t} - 1) + \sqrt{2}, \right.$$
$$\left. \frac{16 - \sqrt{2}\,q_n^2 + 8\sqrt{2}}{2\,q_n} < \frac{s_0}{\sqrt{a}} < \frac{16 + \sqrt{2}\,q_n^2 - 8\sqrt{2}}{2\,q_n} \right\}.$$
$$(9)$$

The net effect of growth does not modify the latter inequalities since they involve the perimeter terms. As noted before, such terms are not affected by growth. Needless to say, for $\alpha_{0t} = 1$ (no growth), Eq. (7) is recovered.

III. VERTEX MODEL SIMULATIONS

To support our findings, and to verify the robustness in non-ideal cases, we implemented a planar vertex model algorithm. Vertex models represent cellular tissues as a plane network of vertices, edges and areas, and associate a potential energy to each cell in the tessellation. Such models have been widely used to describe the evolution of living tissues and are by now a standard tool.

Let $\mathbf{r}_i$ denote the position vector of the ith vertex in the tessellation. Then, the vertex position evolves in time according to the quasistatic motion law

$$\frac{\partial \mathbf{r}_i}{\partial t} = -\frac{1}{\gamma}\frac{\partial E}{\partial \mathbf{r}_i},$$

where t is time, E is the total energy of the tissue [the sum of (1) for all cells in the tissue], and γ is a viscous coefficient. $-\frac{\partial E}{\partial \mathbf{r}_i}$ is the resultant force acting on the ith vertex. We clarify that the implemented cell division algorithm does not take into account effects due to cell elongation in order to keep the algorithm as "clean" as possible and consistent with the

TABLE I. Parameters used for the five synthetic experiments: summary.

	Synthetic experiment				
	1	2	3	4	5
s_0	3.7224	3.7224	3.7224	3.7224	2, 5
K	0.1250	0.0909	0.0909	0.0909	0.1250
α	3.2475	4.1266	4.1266	2.3618	3.2475
p	6.7081	7.9777	7.9777	5.7207	6.7081
Growth	N	N	N	Y	N
Division region	$\mathcal{A}_\infty$	$\mathcal{A}_\infty$	$\alpha > 0.9$	$\mathcal{A}_\infty$	$\mathcal{A}_\infty, \alpha > 0.9$

analytical results. A refined algorithm goes beyond the scope of this work.

The pseudocode of our implementation is shown in Algorithm 1.

Algorithm 1 Vertex model implementation

Require: Initial geometry, parameters
1: Evaluate and store the initial picture of the system
2: **for** $j = 1, \ldots, N_{\text{iter}}$ **do**
3:    Update geometry, parameters
4:    **for** $i = 1, \ldots, N_{\text{cells}}$ **do**
5:       Check for mitosis for the ith cell
6:       **if** Check is satisfied **then**
7:          Divide ith cell
8:       **end if**
9:    **end for**
10:    Update geometry, connectivity, parameters
11:    Evaluate nodal forces
12:    Update vertices position (time integration)
13:    Evaluate and store the picture of the system for the jth iteration
14: **end for**

After a complete initialization, in terms of geometry, connectivity of cells, and various parameters, the code enters in the time loop. For every time iteration, geometry and parameters are updated. Then, the algorithm checks whether cells can be divided, in compliance with some constraint on mitosis [e.g., (7)]. If so, the cell is divided, and the current status of the system is updated. Hence, nodal forces are evaluated, time integration is performed (via a fourth-order explicit Runge-Kutta method), and the vertices position is updated. Meaningful quantities for the continuation of the loop and for the postprocessing phase are evaluated and stored.

We performed five synthetic experiments. For all of them, the animations of the simulations are available in the supplemental material [41]. Table I summarizes the main features and the values of parameters used for the simulations.

The first synthetic experiment considers a regular hexagonal cell in the reference configuration. The vertex model is initialized with the following parameters: $s_0 = 3.7224$, $K = 0.1250$, $\alpha = 3.2475$, $p = 6.7081$ (α and p refer to the area and perimeter ratios of the reference configuration). Division is only allowed when (α, p) is inside $\mathcal{A}_\infty$. The referential and final configurations are shown in Figs. 5(a) and 5(b). The energy evolution for the whole tissue, from the referential
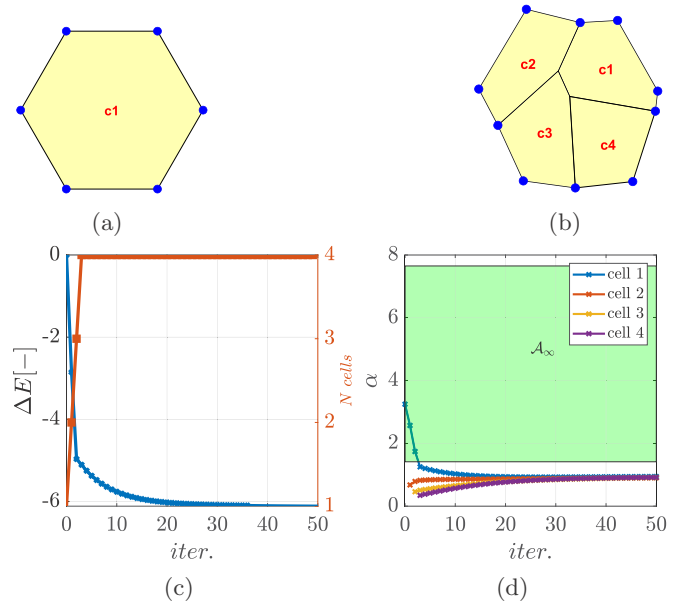

FIG. 5. Numeric simulation results of the first synthetic experiment: regular hexagonal cell, favorable division. (a) Referential configuration; (b) final configuration (full evolution available in the supplemental material [41]); (c) energy difference; (d) area history for every cell (in green the region $\mathcal{A}\infty$).

value, is shown in Fig. 5(c), together with the number of cells for every iteration. It is evident how cell divisions are energetically convenient for the cells. After three divisions, mitosis is no longer energetically favorable. This is confirmed by Fig. 5(d), where the area history for every cell is plotted. As long as cells lie inside $\mathcal{A}_\infty$ (green region in the figure), division decreases the energy of the system.

For the second synthetic experiment, we consider a simple tissue composed by nine cells, which are not regular polygons. We tuned the model as in the previous experiment, except for $\alpha = 4.1266$, $p = 7.9777$, and $K = 0.0909$ (all on average). Division is only allowed when (α, p) is inside $\mathcal{A}_\infty$. Results are shown in Fig. 6. Similarly to the first experiment, as long as cells are permitted to divide within the region $\mathcal{A}_\infty$, the energy of the system decreases. The final configuration contains 34 cells. For the sake of completeness, the area history for every cell is depicted in Fig. 6(d).

The third synthetic experiment shows the effect of uncritical division. To do so, we consider again the setup of the second experiment, but we allow cells to divide regardless of any energetic consideration. To avoid numerical instabilities, we just considered $\alpha = 0.90$ as a threshold for mitosis. Below this limit, mitosis in not permitted. Results are reported in Fig. 7.

For the very first iterations, the energy profile follows that of the second experiment. However, in this experiment cells can divide also when they lie outside the favorable region, thus causing energy to increase. When $\alpha < 0.90$ for every cell, mitosis stops. The final configuration contains 58 cells. As expected, the relaxation of mitosis conditions leads to a higher number of cells. For the sake of completeness, the area history for every cell is depicted in Fig. 7(d).

The fourth synthetic experiment conjugates growth and mitosis. The reference configuration is that of the first synthetic
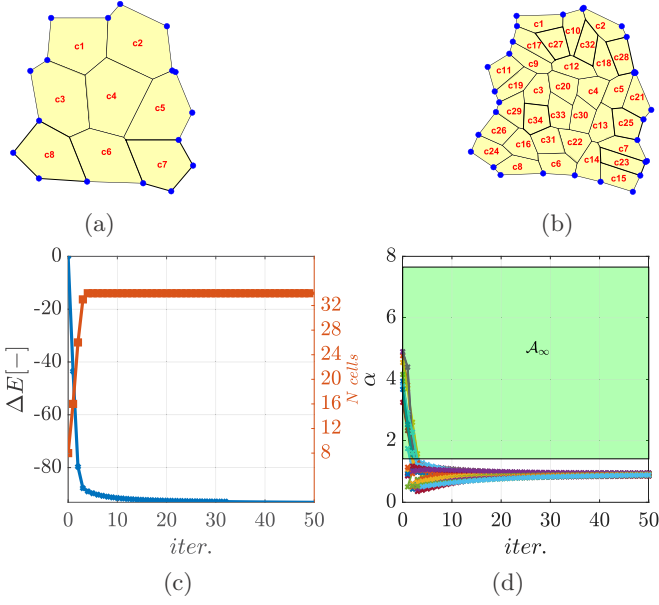
(a)

(b)

(c)

(d)

FIG. 6. Numeric simulation results of the second synthetic experiment: irregular cells, favorable division. (a) Referential configuration; (b) final configuration (full evolution available in the supplemental material [41]); (c) energy difference; and (d) area history for every cell (in the green region $\mathcal{A}_\infty$).

(a)

(b)

FIG. 8. Numeric simulation results of the fourth synthetic experiment: regular cell, favorable division, and growth. (a) Referential configuration; (b) final configuration (full evolution available in the supplemental material [41]); (c) energy difference; (d) area history for every cell.

However, the energy decreases whenever cell division occurs. For the sake of completeness, Fig. 8(d) shows the area history for every cell. The region $\mathcal{A}_\infty$ is not reported, since it changes in time for every cell. The final configuration is composed of 30 cells. This is in contrast with the first experiment, which actually considers only relaxation of the cells up to a level where mitosis is not favorable. The presence of growth clearly sustains proliferation, as can be seen in Fig. 8(c), where the energy evolution is not monotone as in the first experiment, and it presents many spikes (see also the measurements in Fig. 1 of Ref. [35]).

The fifth experiment considers the same setting as that of the first experiment, but s_0 is made to vary. We considered the cases $s_0 = 2, 5$ so as to include situations in which the isoperimetric inequality is not/is satisfied, respectively. For both cases, we report in the odd rows of Fig. 9 the energy evolution and the area history when energetic conditions are taken into account for mitosis, i.e., (7), while in the even rows of the same figure we report the results when uncritical division ($\alpha > 0.9$) is allowed. The effect of introducing energetic considerations is more evident for the case $s_0 = 5$. In fact, looking at Figs. 9(g) and 9(h) we can see how drastically uncritical division increases the energy content of the tissue.

IV. OPTIMAL CELL CYCLE

In this section, we pursue the complete time evolution of a growing cell undergoing division, yet in a particular ideal case. We consider a single, regular, hexagonal cell which realizes, at every instant, the configuration of least energy. When the cell reaches the critical area, i.e., when the cell enters the favorable region for division for the first time, the cell splits into two equal halves. We further suppose that the daughter cells do not grow and relax towards states of least energy.

experiment, but parameters are set as in Table I. We consider the exponential growth law $\alpha_{0t} = (1.01)^{i - i_{\text{app}}}$, where i is the current number of iterations and i_{app} is the iteration where the cell is generated. Mitosis happens whenever parameters lie in $\mathcal{A}_\infty$ [see Eq. (9)]. The effect of monotonic growth is to increase the energy level of the tissue, as shown in Fig. 8(c).
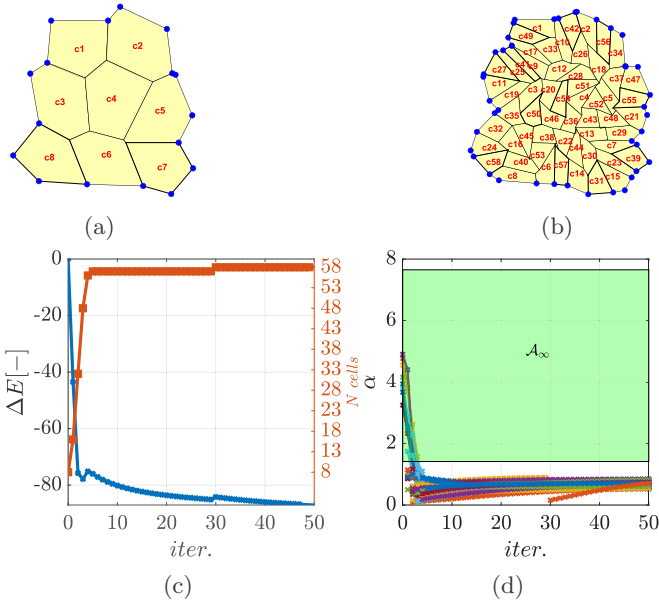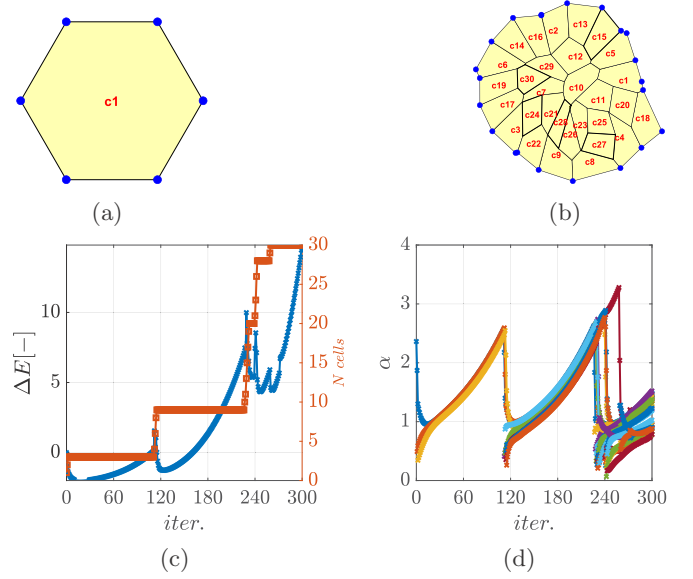

(a)

(b)

(c)

(d)

FIG. 7. Numeric simulation results of the third synthetic experiment: irregular cells, uncritical division. (a) Referential configuration; (b) final configuration (full evolution available in the supplemental material [41]); (c) energy difference; (d) area history for every cell (in the green region $\mathcal{A}_\infty$).
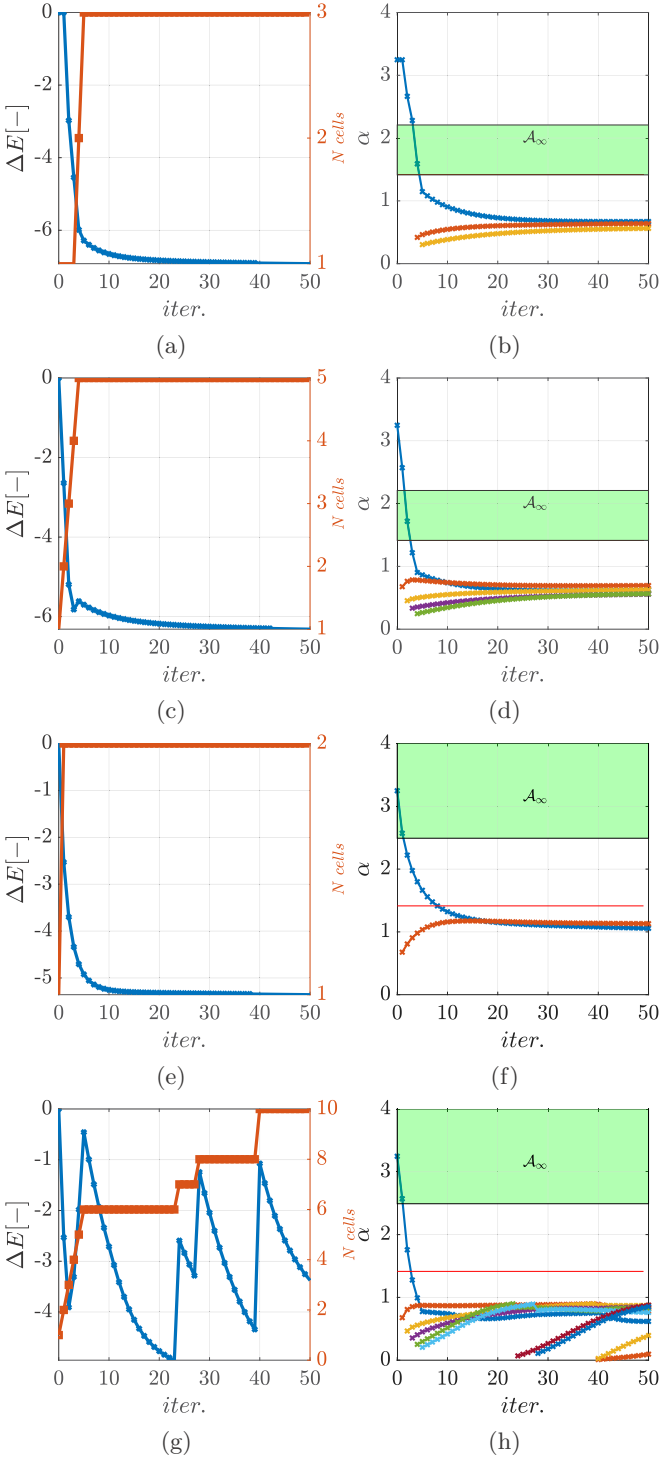
FIG. 9. Numeric simulation results of the fifth synthetic experiment: regular cell, s_0 varies. (a),(b) $s_0 = 2$, favorable division; (c),(d) $s_0 = 2$, uncritical division; (e),(f) $s_0 = 5$, favorable division; (g),(h) $s_0 = 5$, uncritical division. Full evolutions available in the supplemental material [41].

The following result characterizes least energy configurations in a general setting.

Proposition 2. Let $E = (\alpha - \alpha_{0t})^2 + K(p - s_0)^2$ be the energy of a n-gonal, possibly growing, cell. Then, there exists a

unique minimizing pair $(\bar{\alpha}, \bar{p})$ given by

$$(\bar{\alpha}, \bar{p}) = \begin{cases} (\alpha_{0t}, s_0) & \text{if } s_0 > q_n\sqrt{\alpha_{0t}}, \\ (\beta, q_n\sqrt{\beta}) & \text{otherwise}, \end{cases}$$

where $(\frac{s_0}{q_n})^2 < \beta < \alpha_{0t}$ is the unique positive real number satisfying

$$\sqrt{\beta^3} + \left(\frac{Kq_n^2}{2} - \alpha_{0t}\right)\sqrt{\beta} - \frac{q_n s_0 K}{2} = 0. \quad (10)$$

Proof. To be meaningful, the minimization of E must be performed under the constraint of the isoperimetric inequality $\frac{p}{\sqrt{\alpha}} \geqslant q_n$.

We thus consider the Lagrangian $E + \lambda(q_n\sqrt{\alpha} - p)$, where λ is the Lagrange multiplier to enforce the constraint. The stationarity of the Lagrangian (saddle point) requires the following system to be fulfilled:

$$4\sqrt{\alpha^3} + q_n\lambda - 4\alpha_{0t}\sqrt{\alpha} = 0,$$
$$2K(p - s_0) - \lambda = 0,$$
$$q_n\sqrt{\alpha} - p \leqslant 0,$$
$$\lambda \geqslant 0,$$
$$\lambda(q_n\sqrt{\alpha} - p) = 0,$$

or, solving and substituting for λ from the second equation,

$$\begin{aligned} 4\sqrt{\alpha^3} + 2Kq_n(p - s_0) - 4\alpha_{0t}\sqrt{\alpha} &= 0, \\ q_n\sqrt{\alpha} - p &\leqslant 0, \\ p &\geqslant s_0, \\ (p - s_0)(q_n\sqrt{\alpha} - p) &= 0. \end{aligned} \quad (11)$$

From the last of (11), we distinguish two cases.

(i) If $p = s_0$, the constraint is not active ($\lambda = 0$), and we readily deduce $q_n\sqrt{\alpha} < s_0$ and $(\bar{\alpha}, \bar{p}) = (\alpha_{0t}, s_0)$. This case corresponds to the compliance of the isoperimetric inequality. *A fortiori*, the following inequality holds: $q_n\sqrt{\alpha_{0t}} < s_0$. The minimal energy level is $E = 0$.

(ii) If $p = q_n\sqrt{\alpha}$, the constraint is active ($\lambda \neq 0$), and the least-energy configuration is a regular n-gon. We further deduce that $s_0 \leqslant q_n\sqrt{\alpha}$. The first of (11) provides

$$\sqrt{\alpha^3} + \left(\frac{Kq_n^2}{2} - \alpha_{0t}\right)\sqrt{\alpha} - \frac{q_n s_0 K}{2} = 0.$$

By the Descartes-Laguerre rule of sign [37], we easily deduce that the equation admits just one positive real root, say β, regardless of the sign of $(\frac{Kq_n^2}{2} - \alpha_{0t})$.

We claim that $(\frac{s_0}{q_n})^2 < \beta < \alpha_{0t}$. The number of positive real roots greater than α_{0t} is linked to the sign alternances of $\{1, \frac{Kq_n^2\sqrt{\alpha_{0t}}}{2}, \frac{Kq_n}{2}(q_n\sqrt{\alpha_{0t}} - s_0)\}$ (see Ref. [37], Prop. p. 102). In this regime, $s_0 \leqslant q_n\sqrt{\alpha_{0t}}$, and there are no sign alternances. Similarly, the number of positive real roots less than $(\frac{s_0}{q_n})^2$ is linked to the sign alternances of $\{-\frac{q_s s_0 K}{2}, -\frac{s_0\alpha_{0t}}{q_n}, -\frac{s_0}{q_n}(\alpha_{0t} - (\frac{s_0}{q_n})^2)\}$ (see Ref. [37], Prop. p. 106). Again, being $s_0 \leqslant q_n\sqrt{\alpha_{0t}}$, there are no sign alternances, and the thesis is proved.

The most interesting case to be studied is the incompatible regime $s_0 \leqslant q_n\sqrt{\alpha_{0t}}$. Since a closed form solution to (10) cannot be found, we performed a simple computation
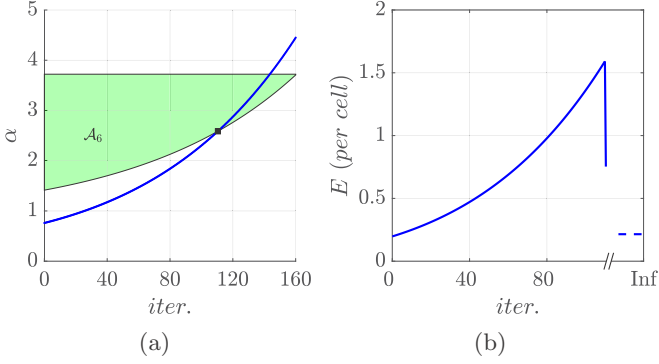
FIG. 10. Time evolution of a least-energy regular, hexagonal cell. (a) Area history; (b) energy history per cell (after cell division, the energy of one of the daughter cells is reported).

with the following parameters: $n = 6$, $K = 0.1$, $s_0 = 2$, $\alpha_{0t} = (1.01)^{i-i_{app}}$. Results are shown in Fig. 10. Figure 10(a) shows the favorable division region $\mathcal{A}_6$ [Eq. (9)] and the evolution of the current area (blue curve) as a solution of (10). The black square marker highlights the critical values of area and time when, for the first time, the cell finds division advantageous. Figure 10(b) shows the history of the energy of one cell (after cell division, the energy of one daughter cell is reported). Up to the critical time, energy increases exponentially due to the form of the growth law. When mitosis occurs, the energy of one daughter cell instantaneously reads $E_2 = (\frac{\alpha_{cr}}{2} - 1)^2 + K(\frac{q_6\sqrt{\alpha_{cr}}}{2} + \frac{4\sqrt{\alpha_{cr}}}{q_6} - s_0)^2$. If the pentagonal daughter cells do not growth, after some amount of time, possibly infinite, the system reaches a relaxed configuration characterized by two regular, pentagonal cells (note that $s_0 < q_5$). The final area and energy, for one daughter cell, are given by the solution of the following system:

$$\sqrt{\alpha^3} + \left(\frac{Kq_5^2}{2} - 1\right)\sqrt{\alpha} - \frac{q_5 s_0 K}{2} = 0,$$

$$E = (\alpha - 1)^2 + K(q_5\sqrt{\alpha} - s_0)^2.$$

Such an energy level is represented by a dashed line in Fig. 10(b). It is slightly higher than the maternal one due to the presence of q_5 instead of q_6. The trend is consistent with the experimental observations already reported in Sec. I.

V. DISCUSSION AND CONCLUSIONS

We addressed the question of whether cell division is energetically favorable or not, and whether we can identify the cases. Unlike T1 and glassy-fluid transitions, we showed that cell division is not ruled by a single parameter (the target shape index [1]), but that the interplay between actual and target geometrical ratios and cells elasticity is more involved and far from trivial. We discovered that the energetic convenience region for mitosis can be expressed in terms of the ratio between initial and target areas, and in terms of the target shape parameter. The effect of cells elasticity saturates as the cells become more and more compressible. In addition, we derived exact expressions for a domain where division is

energetically favorable, i.e., a region unaffected by the level of compressibility and by the number of sides. Furthermore, we quantified the effect of unequal cell division. We found that this effect is weak, at least for nonpathological cases in which the daughter cells have very different areas. Finally, we characterized lowest-energy configurations, and we simulated a complete, ideal cell cycle. The validity of the theoretical results has been supported by many synthetic experiments using a vertex model method approach. Results have been found to be consistent with theoretical expectations.

We expect that our findings may be of interest to a wide class of scientists. We show under which conditions mitosis is energetically favorable for the cell. Our results may shed light on the energetics of actual cells mitosis and on more complex biological phenomena correlated to proliferation, such as tumor growth and the evolution of competing cells. In fact, our results can be easily implemented in vertex model algorithms, thus they will enhance the reliability and likelihood of these tools. This is an important factor in computational biology. Moreover, results are consistent with the well-documented tendency of tumors to be fluidlike [38]: we found that the domain where cell division is favorable extends more in the fluidlike region. We suppose there is a deeper connection between malignant cell unregulated proliferation and the parameters ruling the energetics of cell division. In some cases, division must be sustained by some energy supply, while in others it is energetically favorable and occurs spontaneously. It is worthwhile to investigate if a converse statement holds true, namely if malignant cells can only lie inside the convenience region, and thus to provide a precise mechanical characterization of those cells. The connection between malignant cell behavior and elasticity is, after all, accurately documented [17,36,38–40]. It is also well known that in malignant cells, the feedback regulating the internal stress level and growth is compromised [19]. In light of these observations, we speculate about the possibility that the malfunctioning feedback effect is bringing cells to lie within the convenience region for division by altering the target area and/or the target shape index, or by acting on the elastic moduli.

In addition, the results offer a cell characterization, from a geometrical-mechanical viewpoint, that potentially opens new perspectives. The hypothesis about the characterization of malignant cell functioning, through an altered internal feedback mechanism that makes the cells behave as though they are in the favorable region, may pave the way for a new experimental research topic to confirm such an idea. Thus, by measuring the geometrical and elastic properties of the cell, one could detect malignant cells from among others. That is the starting point for a better understanding of cancer. Moreover, this may have an impact not only for academics, but also for physicians, for instance to develop better strategies for cancer treatment.

ACKNOWLEDGMENTS

[1] D. Bi, J. H. Lopez, J. M. Schwarz, and M. L. Manning, A density-independent rigidity transition in biological tissues, Nat. Phys. **11**, 1074 (2015).

[2] P. Sahu, J. Kang, G. Erdemci-Tandogan, and M. L. Manning, Linear and nonlinear mechanical responses can be quite different in models for biological tissues, Soft Matter **16**, 1850 (2020).

[3] D. B. Staple, R. Farhadifar, J. C. Röper, B. Aigouy, S. Eaton, and F. Jülicher, Mechanics and remodelling of cell packings in epithelia, Eur. Phys. J. E **33**, 117 (2010).

[4] D. Bi, J. H. Lopez, J. M. Schwarz, and M. Lisa Manning, Energy barriers and cell migration in densely packed tissues, Soft Matter **10**, 1885 (2014).

[5] D. Bi, X. Yang, M. C. Marchetti, and M. L. Manning, Motility-Driven Glass and Jamming Transitions in Biological Tissues, Phys. Rev. X **6**, 021011 (2016).

[6] A. Hernandez, M. F. Staddon, M. J. Bowick, M. C. Marchetti, and M. Moshe, Anomalous elasticity of a cellular tissue vertex model, Phys. Rev. E **105**, 064611 (2022).

[7] R. Kupferman, B. Maman, and M. Moshe, Continuum mechanics of a cellular tissue model, J. Mech. Phys. Solids **143**, 104085 (2020).

[8] A. DiCarlo and S. Quiligotti, Growth and balance, Mech. Res. Commun. **29**, 449 (2002).

[9] D. Ambrosi and F. Mollica, On the mechanics of a growing tumor, Int. J. Eng. Sci. **40**, 1297 (2002).

[10] M. Epstein and G. A. Maugin, Thermomechanics of volumetric growth in uniform bodies, Int. J. Plast. **16**, 951 (2000).

[11] A. Goriely, *The Mathematics and Mechanics of Biological Growth*, Interdisciplinary Applied Mathematics, Vol. 45 (Springer, New York, 2017), pp. 1–66.

[12] M. Soleimani, N. Muthyala, M. Marino, and P. Wriggers, A novel stress-induced anisotropic growth model driven by nutrient diffusion: Theory, FEM implementation and applications in bio-mechanical problems, J. Mech. Phys. Solids **144**, 104097 (2020).

[13] W. Noll, Materially uniform simple bodies with inhomogeneities, Arch. Ration. Mech. Anal. **27**, 1 (1967).

[14] E. K. Rodriguez, A. Hoger, and A. D. McCulloch, Stress-dependent finite growth in soft elastic tissues, J. Biomech. **27**, 455 (1994).

[15] A. Yavari, A geometric theory of growth mechanics, J. Nonlinear Sci. **20**, 781 (2010).

[16] J. Folkman and M. Hochberg, Self-regulation of growth in three dimensions, J. Exp. Med. **138**, 745 (1973).

[17] M. Basan, T. Risler, J. F. Joanny, X. Sastre-Garau, and J. Prost, Homeostatic competition drives tumor growth and metastasis nucleation, HFSP J. **3**, 265 (2009).

[18] R. Levayer, Solid stress, competition for space and cancer: The opposing roles of mechanical cell competition in tumour initiation and growth, Seminars Cancer Biol. **63**, 69 (2020).

[19] D. Ambrosi, S. Pezzuto, D. Riccobelli, T. Stylianopoulos, and P. Ciarletta, Solid tumors are poroelastic solids with a chemo-mechanical feedback on growth, J. Elast. **129**, 107 (2017).

[20] A. Nestor-Bergmann, G. Goddard, S. Woolner, and O. E. Jensen, Relating cell shape and mechanical stress in a spatially disordered epithelium using a vertex-based model, Math. Med. Biol. **35**, i1 (2018).

[21] A. G. Fletcher, M. Osterfield, R. E. Baker, and S. Y. Shvartsman, Vertex models of epithelial morphogenesis, Biophys. J. **106**, 2291 (2014).

[22] D. L. Barton, S. Henkes, C. J. Weijer, and R. Sknepnek, Active Vertex Model for cell-resolution description of epithelial tissue mechanics., PLOS Computational Biology **13**, e1005569 (2017).

[23] J. Huang, J. O. Cochran, S. M. Fielding, M. C. Marchetti, and D. Bi, Shear-Driven Solidification and Nonlinear Elasticity in Epithelial Tissues, Phys. Rev. Lett. **128**, 178001 (2022).

[24] A. G. Fletcher, J. M. Osborne, P. K. Maini, and D. J. Gavaghan, Implementing vertex dynamics models of cell populations in biology within a consistent computational framework, Prog. Biophys. Mol. Biol. **113**, 299 (2013).

[25] G. W. Brodland and J. H. Veldhuis, Computer simulations of mitosis and interdependencies between mitosis orientation, cell shape and epithelia reshaping, J. Biomech. **35**, 673 (2002).

[26] G. I. Bell and E. C. Anderson, Cell growth and division: I. A mathematical model with applications to cell volume distributions in mammalian suspension cultures, Biophys. J. **7**, 329 (1967).

[27] R. Farhadifar, J. C. Röper, B. Aigouy, S. Eaton, and F. Jülicher, The influence of cell mechanics, cell-cell interactions, and proliferation on epithelial packing, Curr. Biol. **17**, 2095 (2007).

[28] Y. Li, H. Naveed, S. Kachalo, L. X. Xu, and J. Liang, Mechanisms of regulating cell topology in proliferating epithelia: Impact of division plane, mechanical forces, and cell memory, PLoS One **7**, e43108 (2012).

[29] C. Guillot and T. Lecuit, Mechanics of epithelial tissue homeostasis and morphogenesis, Science **340**, 1185 (2013).

[30] M. Czajkowski, D. M. Sussman, M. C. Marchetti, and M. L. Manning, Glassy dynamics in models of confluent tissue with mitosis and apoptosis, Soft Matter **15**, 9133 (2019).

[31] A. Merzouki, O. Malaspinas, A. Trushko, A. Roux, and B. Chopard, Influence of cell mechanics and proliferation on the buckling of simulated tissues using a vertex model, Natural Comput. **17**, 511 (2018).

[32] M. Salazar-Roa and M. Malumbres, Fueling the Cell Division Cycle, Trends Cell Biol. **27**, 69 (2017).

[33] K. J. Barnum and M. J. O'Connell, Cell cycle regulation by checkpoints, Methods Molec. Biol. **1170**, 29 (2014).

[34] R. Phillips, J. Kondev, J. Theriot, H. G. Garcia, and N. Orme, *Physical Biology of the Cell*, 2nd ed. (Garland Science, London and New York, 2012), Vol. 78, pp. 1230–1230.

[35] J. H. Kang, G. Katsikis, Z. Li, K. M. Sapp, M. A. Stockslager, D. Lim, M. G. Vander Heiden, M. B. Yaffe, S. R. Manalis, and T. P. Miettinen, Monitoring and modeling of lymphocytic leukemia cell bioenergetics reveals decreased ATP synthesis during cell division, Nat. Commun. **11**, 4983 (2020).

[36] V. F. Fiore, M. Krajnc, F. G. Quiroz, J. Levorse, H. A. Pasolli, S. Y. Shvartsman, and E. Fuchs, Mechanics of a multilayer epithelium instruct tumour architecture and function, Nature (London) **585**, 433 (2020).

[37] E. Laguerre, Mémoire sur la théorie des équations numériques, J Math. Pures Appl. **9**, 99 (1883).

[38] Y. L. Han, A. F. Pegoraro, H. Li, K. Li, Y. Yuan, G. Xu, Z. Gu, J. Sun, Y. Hao, S. K. Gupta, Y. Li, W. Tang, H. Kang, L. Teng, J. J. Fredberg, and M. Guo, Cell swelling, softening and invasion in a three-dimensional breast cancer model, Nat. Phys. **16**, 101 (2020).

[39] P. Guo, D. Liu, K. Subramanyam, B. Wang, J. Yang, J. Huang, D. T. Auguste, and M. A. Moses, Nanoparticle elasticity directs tumor uptake, Nat. Commun. **9**, 130 (2018).

[40] O. Chaudhuri, S. T. Koshy, C. Branco Da Cunha, J. W. Shin, C. S. Verbeke, K. H. Allison, and D. J. Mooney, Extracellular matrix stiffness and composition jointly regulate the induction of malignant phenotypes in mammary epithelium, Nat. Mater. **13**, 970 (2014).

[41] See Supplemental Material at http://link.aps.org/supplemental/ 10.1103/PhysRevE.106.054405 for the animations of the numerical experiments.